ORIGINAL PAPER

Effect of nano-silica on mechanical properties and microstructure of high-volume ground granulated blast furnace slag cement paste

Qinqiang Wang[1] · Kangbing Ma[2] · Tao Liu[1]

Abstract

Incorporating ground granulated blast furnace slag (GBS) as a supplementary cementitious material in cementitious materials can reduce the cement content and improve the performance of cement-based materials. However, adding GBS especially in large quantities, tends to decrease the early-age performance of cement-based materials, such as reducing early strength, increasing porosity, etc. This study introduced nanosilica (NS) into cementitious materials with a high volume GBS to address the deficiencies in early-age performance. This study aims to investigate and discuss the influence of NS on the mechanical properties and microstructure of cementitious materials with a high-volume GBS. The compressive strength, composition of hydration products, distribution of pores, composition of pore structure and microscopic morphology were tested and analyzed. Results showed a significant strength reduction in high-volume GBS (60 wt% GBS) cement paste when compared with pure cement paste samples. NS demonstrated a remarkable enhancement in the strength of high-volume GBS-contained samples in 3 and 7 days. The positive impact of NS on the strength of high-volume GBS-contained samples remained evident at 28 days of age. NS facilitated the hydration of C_3S and C_2S in high-volume GBS-contained samples. The enhancement in the hydration percentage of C_2S was particularly pronounced. In the high-volume GBS-containing cementitious materials, NS continued to consume CH and participate in pozzolanic reactions at a later age. NS decreased the pore volume in the ranges of >100 μm and 100 nm–1 μm in high-volume GBS-contained samples, reduced the quantity of unhydrated GBS and resulted in a more compact structure. The enhancement of strength and the promotion of C_3S and C_2S hydration in increased with the higher addition of NS at 1 wt% and 2 wt%. However, this enhancement and promotion effect diminished when the NS dosage increased to 3 wt%.

Graphical Abstract

Cumulative pore volume of cement paste samples at curing age of (a) 7 days and (b) 28 days.
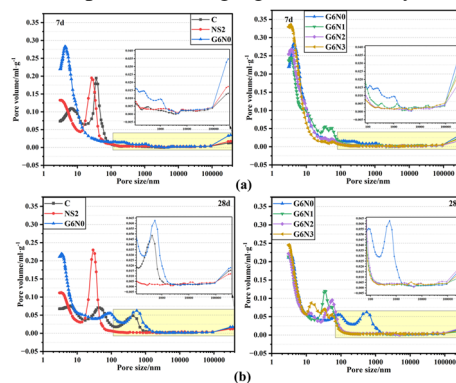
✉ Kangbing Ma
tyhnt1@126.com

1   Qingdao University of Technology, Linyi 276000, China

2   Linyi Vocational University of Science and Technology, Linyi 276000, China

Highlights

- Nano-silica significantly enhanced the strength of high-volume GBS-contained samples at early and late age.
- The enhancement in the hydration percentage of C_2S was particularly pronounced in high-volume GBS cementitious materials with nano-silica addition.
- The influence of nano-silica on the pore structure of the pure cementitious system diminished, whereas it remained prominent in high-volume GBS cement paste.

1 Introduction

Cement-based materials, as one of the primary construction materials, are extensively utilized in infrastructure projects and large-scale constructions. The usage of cement-based materials is enormous, and the consumption of cement itself is also substantial [1, 2]. According to statistics, in 2022, China's cement production reached 2.13 billion tons, maintaining its position as the world's top producer, with India ranking second at 384 million tons [3]. In 2022, China's concrete production reached 3.452 billion cubic meters, indicating a substantial demand and consumption of cement in the country [4]. Cement production involves high-temperature calcination and the decomposition of minerals, resulting in a significant release of CO_2. Approximately 0.6–0.9 tons of CO_2 were emitted for every ton of cement produced. Therefore, cement production entails substantial resource consumption, environmental pollution, and the release of greenhouse gases, contributing to global warming. Ground granulated blast furnace granulated slag (GBS) is a by-product of iron production in pig-iron production. Its primary chemical composition includes CaO, SiO_2, and Al_2O_3; its main mineral phase is the vitreous phase. Approximately 0.14 tons of carbon dioxide are emitted for every ton of GBS produced [5]. Due to its production process and composition, GBS exhibits hydraulic reactivity and is widely used as a supplementary cementitious material in cement-based materials. It is employed to replace cement partially, reducing the overall cement consumption and improving the performance of cement-based materials [6–10]. The hydration of GBS in cement primarily involves the dissolution of its vitreous phase and the reaction with calcium hydroxide ($Ca(OH)_2$, CH) generated from cement hydration, leading to the formation of the C-S-H gel [11].

However, the hydration reactivity of GBS is lower than that of cement. Research has indicated that the appropriate incorporation of GBS to replace cement can enhance the performance of cement-based materials [12]. The study by Ozturk et al. [6] indicated that increasing the GBS content from 10% to 30% increased the compressive strength of the mortars at a curing age of 28 days. Similar results were also found in the research by Choi et al. [13]. At the same time, Choi et al. [13] observed that adding 35 wt% and 50 wt% GBS significantly reduced the porosity of cement paste at the 28-day curing age. Li et al. [14] found that incorporating 5–35wt% GBS as part of the cementitious material reduced the chloride ion transport properties of cementitious materials, increased strength, reduced porosity, and improved resistance to sulfate attack. It can be seen that the addition of an appropriate amount of GBS significantly improved the performance of cementitious materials. However, GBS has an adverse effect on the early performance of cementitious materials [7]. Meanwhile, when the content of GBS increased especially exceeds to 50 wt%, it also has a negative impact on the performance of cementitious materials [15–18]. Due to its low reactivity, GBS can lead to insufficient early strength, porous structure, and increased transport properties of cementitious materials [19]. The study by Ozturk et al. [6] indicated that due to the insufficient early reactivity of GBS, increasing the GBS content in mortars resulted in a decrease in 7-day compressive strengths. In the research conducted by Cheol Choi et al. [13], it was found that with the increase in GBS content, the 3-day strength of cementitious materials was significantly insufficient, and the porosity increased significantly. Sanjuán et al. [20] found that due to the insufficient early reactivity of added GBS, the use of a large amount of GBS led to a porous structure, resulting in an increase in carbonation rate and with a decrease in curing time the degree of carbonation increased. Therefore, it is necessary to find a way to compensate for the negative impact of GBS on the performance of cementitious materials while increasing the substitution of GBS, in order to reduce cement consumption and achieve the goal of reducing energy consumption and carbon emissions.

Nanosilica (NS), as a type of nanomaterial, has been widely utilized in recent years for enhancing the performance of cementitious materials, especially in terms of early-age properties [21–26]. Studies have demonstrated that even in small quantities, NS can facilitate the early hydration of cement [27], acting as a nucleation site for the

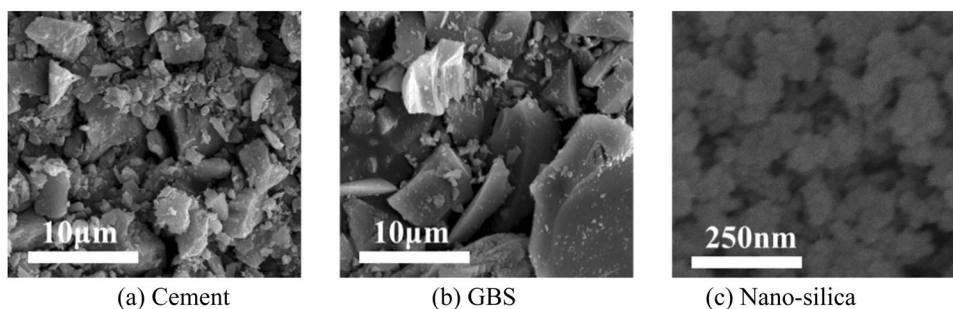**Fig. 1** Microscopic morphology of raw materials (**a**) cement, (**b**) ground granulated blast furnace slag and (**c**) nanosilica

(a) Cement

(b) GBS

(c) Nano-silica

Table 1 Chemical compositions of raw materials (*wt.%*)

Sample	CaO	SiO$_2$	Al$_2$O$_3$	SO$_3$	MgO	K$_2$O	Fe$_2$O$_3$	LOI
GBS	43.87	26.11	10.27	3.05	6.78	0.67	3.99	3.25
Cement	61.52	19.87	5.32	3.78	2.07	0.25	3.15	2.55

growth of C-S-H gel [28]. Additionally, NS can react with CH produced during the early hydration of cement, generating extra C-S-H gel in the early stages [29], thereby enhancing early strength [30], promoting a dense pore structure, and improving pore composition [31]. The presence of NS in the cementitious materials reduces the calcium-silica ratio of the C-S-H gel, resulting in enhanced resistance to decalcification under erosion conditions [32, 33]. Studies by Guo et al. [34, 35] have shown that the addition of NS in cement paste reduced the post-hydration content of CH, densified the pore structure and impeded the transport in cement paste under sulfate attack. Singh et al. [36, 37] found that NS can accelerate the hydration rate of tricalcium silicate (C$_3$S) in cement and the growth rate of hydration products by increasing nucleation sites for C-S-H gel. Dolado et al. [38] through their investigation of Belite cement pastes, observed that the addition of NS promotes the hydration of belite, resulting in the formation of highly polymerized C-S-H gel. Hou and Wang et al. [39] suggested that NS promotes the hydration of C$_3$S while simultaneously delaying the hydration process of C$_3$A in cement-based materials. Barbhuiya et al. [21] and Norhasri et al. [24] summarized the effects of NS in cement concrete. They found that using NS increased the early strength of cement-based materials, reduced the content of hydration product CH, increased the content of C-S-H gel, lowered the porosity, and decreased the content of deleterious pores in most studies.

To sum up, the addition of NS has been shown to enhance the early strength of cement-based materials significantly, densify the pore structure, and reduce transport properties. On the other hand, incorporating high-volume GBS leads to insufficient early strength, a porous structure and increased transport properties in cement-based materials. The question arises whether introducing NS into

cementitious materials with a high volume GBS content can address the issue of inadequate early strength and improve pore composition. This study aims to investigate and discuss the influence of NS on the mechanical properties and microstructure of cementitious materials with a high-volume GBS. Meanwhile, to establish a basis for determining the maximum amount of GBS (as a replacement for cement) in the NS-GBS blended cementitious system where nano-silica can compensate for strength loss. The study involved testing and analyzing cement paste samples at various ages, focusing on strength, composition of hydration products, distribution of pores, composition of pore structure, microscopic morphology, and other relevant factors. The goal is to elucidate the impact of NS on the cementitious system with a high volume GBS, understand the underlying mechanisms and subsequently enhance the usage volume of GBS in cement-based materials while reducing cement consumption.

2 Experimental

2.1 Materials

The cement used in this study is PI reference cement (Portland cement of Chinese P·I 42.5 produced by equivalent to European CEM I 42.5), obtained from the China Building Materials Academy, with a specific surface area of 390 m^2/kg. The high-volume ground granulated blast furnace slag (GBS) used is S95 grade, following the GB/T18046-2008 standard [40], and has a specific surface area of 350 m^2/kg. The hydrophilic nanosilica (NS) dry powder used has a specific surface area of 300 m^2/g with a particle size range 7–40 nm and was purchased from China Micron Limited. The microscopic morphology of the raw materials is shown in Fig. 1. It can be observed that both cement and GBS are irregular angular particles, while NS consists of aggregated spherical particles. The chemical composition of cement and slag is presented in Table 1, revealing highest content of CaO in both cement and slag, followed by SiO$_2$. Additionally, the Al$_2$O$_3$ content in GBS is higher than that in cement.

Table 2 Mix proportions of prepared samples (*wt.*%)

Series	Cement	GBS	Nano-silica	w/b
C	100	0	0	0.4
NS2	98	0	0	0.4
G6N0	60	40	0	0.4
G6N1	59	40	1	0.4
G6N2	58	40	2	0.4
G6N3	57	40	3	0.4

2.2 sample preparation

Cement paste samples were prepared for strength testing and microscopic structure analysis, and the mix proportions are detailed in Table 2. During sample preparation, NS was initially subjected to ultrasonic dispersion at a power of 200 W in mixing water for 8 min. Subsequently, the mixing water and powder were thoroughly mixed for 6 min. After completion of mixing, the paste was filled into molds with dimensions of $4 \times 4 \times 4$ cm and subjected to standard curing at 20 °C and ≥95% relative humidity for 1 day. Following curing, the samples were de-molded and further cured in the standard environment for several days before testing.

2.3 Test methods

2.3.1 Compressive strength and change ratio

The strength of the cement paste was assessed using the YAW-3000D microcomputer-controlled electro-hydraulic servo pressure testing machine, with a testing speed controlled at 2.4 kN/s. The average strength value was determined by testing six paste samples. Strength testing was conducted at 3 days, 7 days, and 28 days. The strength change ratio for different samples at various curing ages was calculated using the following formula.

$$F_T = \frac{C_T - C_{CT}}{C_{CT}} \times 100 \tag{1}$$

$$F_{NT} = \frac{C_{NT} - C_{GT}}{C_{GT}} \times 100 \tag{2}$$

Where F_T is the strength change rate for samples with individually added NS or GBS, expressed in %; C_T is the strength of Control group samples at age T, measured in MPa; C_{CT} is the strength of samples with individually added NS or GBS at age T, measured in MPa; F_{NT} is the strength change rate relative to samples with individually added GBS for samples with GBS and NS, expressed in %; C_{NT} is the strength of samples with GBS and NS at age T, measured in MPa; C_{GT} is the strength of samples with individually added GBS at age T, measured in MPa.

The compressive strength changes of cement paste samples at different curing age intervals of F_I was calculated using the following formula.

$$F_I = \frac{C_X - C_Y}{C_Y} \times 100 \tag{3}$$

Where C_X and C_Y represent the strength at curing ages X and Y, measured in MPa, with X and Y taking values of 3, 7, or 28.

2.3.2 Mercury intrusion porosimetry (MIP)

Automatic mercury porosimeter (AutoporeV9620) are used to test the pore structure and porosity of samples cured for 7 and 28 days. The samples were cracked into small pieces and terminally hydrated in alcohol for 72 h, then dried in a vacuum oven at 45 °C for 56 h. MIP tests pore sizes in the range of 3 nm–400 μm. The pore size distribution, porosity, cumulative pore volume and fraction are calculated and presented.

2.3.3 Quantification of hydrated and unhydrated products

Quantitative analysis of hydrated and unhydrated products in cement paste after hydration was performed using X-ray diffraction (XRD). The samples were first dried in a vacuum oven at 45°C for 72 h and then ground into powder below 75 μm using an agate mortar. To calibrate the content of each phase in the hydration system, 10 wt% corundum (α-Al_2O_3) was added uniformly to the sample powder. XRD scans were conducted in the 5–65° range, with a step size of 0.02° and a step time of 0.4 s. The obtained XRD data were subjected to qualitative phase analysis using Jade software (for example, see Fig. 2a), and quantitative analysis was performed using TOPAS software to determine the content of each phase. The fitted curves after TOPAS quantification are shown as an example in Fig. 3, demonstrating good quantification of phases such as unhydrated, hydrated, and amorphous phases in the hydration system.

3 Results and discussions

3.1 Compressive strength

The strength and strength change rates of cement paste samples with different ratios are shown in Fig. 2a, b, respectively. In Fig. 2a, it can be observed that the strength of all samples increases with the increase in curing time. For samples cured for 3 days, the NS2 sample has the highest strength of 48.4 MPa and showed a 16.1% improvement compared to the C sample. This result was attributed to the higher pozzolanic reactivity of NS, which reacted with the
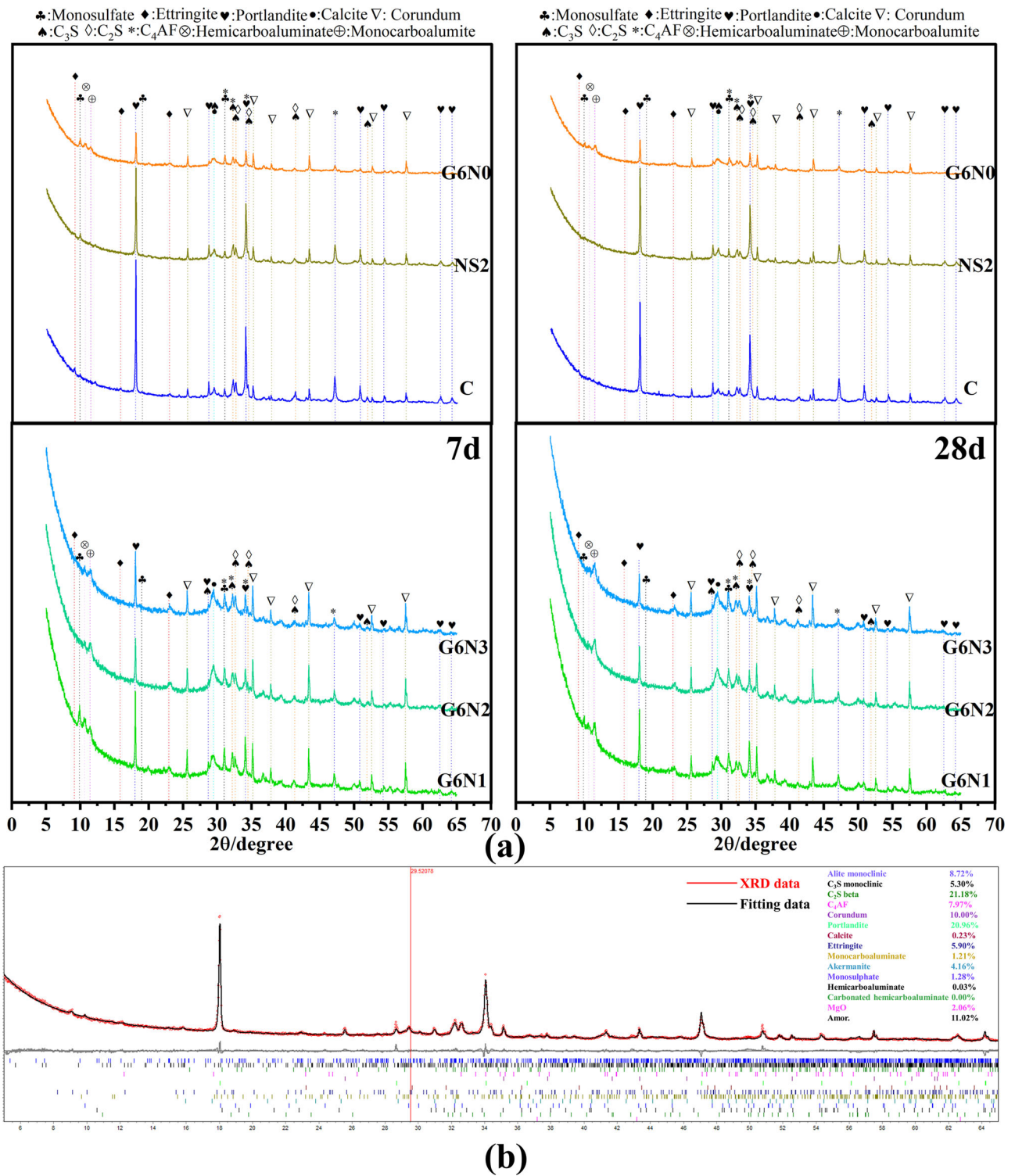
Fig. 2 Quantitative analysis of hydration products with **a** XRD results by **b** TOPAS software

hydrated CH in cement to generate additional C-S-H gel, thereby enhancing the strength. Additionally, the nano-size of NS exhibited a nucleation effect, promoting the hydration of cement [21]. The G6N0 sample has the lowest strength at

27.6 MPa, which was attributed to the lower reactivity of GBS in the early stages of hydration [15]. Moreover, due to the lower cement content, the formation of C-S-H gel was limited, leading to a significant reduction in strength. Similar
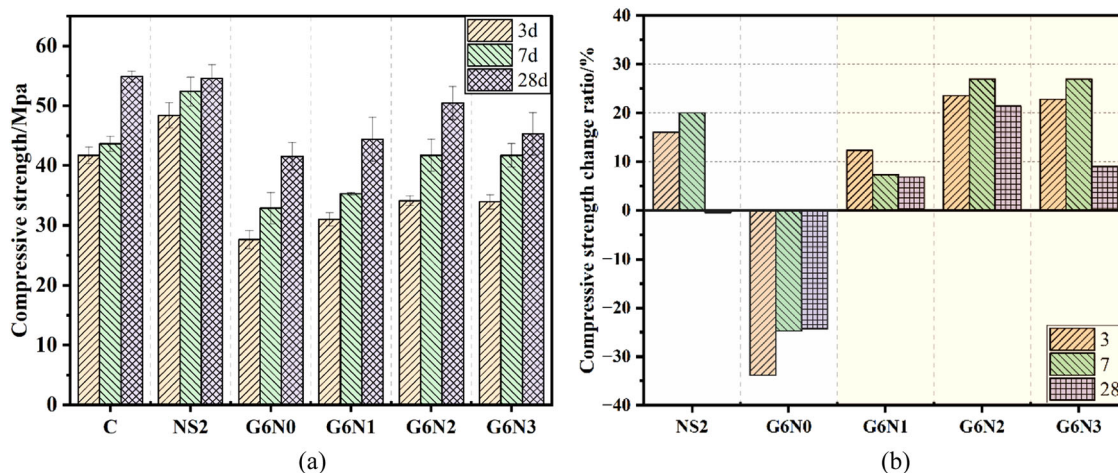
Fig. 3 Compressive strength **a** and compressive strength change ratio **b** of cement paste samples at different curing ages (strength change of the G6N0 sample was relative to the C sample, G6N1, G6N2, and G6N3 samples were relative to the G6N0 sample)

results were revealed by other researchers [17, 18]. The strengths of the G6N1, G6N2, and G6N3 samples were higher than that of the G6N0 sample, measuring 31.0 MPa, 34.1 MPa, and 33.9 MPa, respectively. These values represented strength improvements of 12.3%, 23.6%, and 22.8% relative to the G6N0 sample. This was attributed to the early high reactivity of NS, which enhanced the reactivity of the 60 wt% GBS cementitious system, leading to increased strength. The strength improvement gradually increases as the NS content increases to 2 wt%, but the strength enhancement decreases for the 3 wt% NS sample. This was because a larger amount of NS with poor dispersibility impedes the hydration process by encapsulating some unhydrated particles, reducing the effectiveness of strength enhancement. As the curing age extended to 7 days, the NS2 sample continued to exhibited the highest strength among all samples, measuring 52.4 MPa, representing a strength growth rate of 20.1% relative to the C sample. This result was attributed to the substantial presence of the C-S-H gel, which mainly contributed to strength in the NS2 sample. The higher content of the amorphous phase in the NS2 sample, as quantified by XRD in Fig. 5, confirmed this observation. The G6N0 sample had the lowest strength, containing a higher amorphous phase than NS2 in Fig. 5. This was because GBS predominantly consists of amorphous phases [7, 8], and the 60 wt% GBS increased the amorphous phase content in the composite system rather than the C-S-H gel content. The strengths of G6N1, G6N2, and G6N3 samples were 35.3 MPa, 41.7 MPa, and 41.7 MPa, respectively, higher than the G6N0 strength of 32.9 MPa, representing strength enhancements of 7.3%, 26.9%, and 26.9%. Additionally, the comparison of amorphous phase content in Fig. 5 revealed that G6N1, G6N2, and G6N3 had higher contents than G6N0. This indicated that NS continued to enhance the C-S-H gel content and strength in the 60 wt% GBS system at the 7-day age.

As the curing age extended to 28 days, the C and NS2 samples exhibited similar strengths, measuring 54.9 MPa and 54.6 MPa, respectively. This result was because NS was nearly depleted in the late hydration stage, and its role in enhancing strength was not prominent. Both C and NS2 samples also exhibited similar contents of the amorphous phase in Fig. 5. The strengths of G6N1, G6N2, and G6N3 samples were 44.4 MPa, 50.5 MPa, and 45.3 MPa, respectively, and which was higher than the G6N0 strength of 41.6 MPa, representing strength enhancements of 6.9%, 21.4%, and 9.0%. NS continued to enhance the strength of the 60 wt% GBS cementitious system even at 28 days of hydration, and the amorphous phase content in G6N1, G6N2, and G6N3 samples was higher than that in the G6N0 sample, as indicated in Fig. 5. This suggested that NS has significantly different impacts and durations on the strength of pure cement and high-volume GBS systems. In the late hydration period, NS could still markedly enhance the strength of high-volume GBS systems, while in pure cement systems strength enhancement was mainly observed in the early stages.

Figure 3b represents the strength change rate of cement paste. The addition of NS significantly increased the strength of pure cement and high-volume GBS systems at 3 and 7 days of age. However, as the age extended to 28 days, the strengthening effect of NS on pure cement systems diminished, while the strength increase in high-volume GBS systems persisted. When the NS dosage increased to 2 wt%, the strength enhancement increased with the dosage but decreased when the dosage reached 3 wt%. This was attributed to a higher NS content that may encase around unhydrated particles, impeding react with water for hydration reactions [28, 41, 42].

Figure 4 depicts the strength change rates of cement paste samples during the 3–7 days and 7–28 days curing
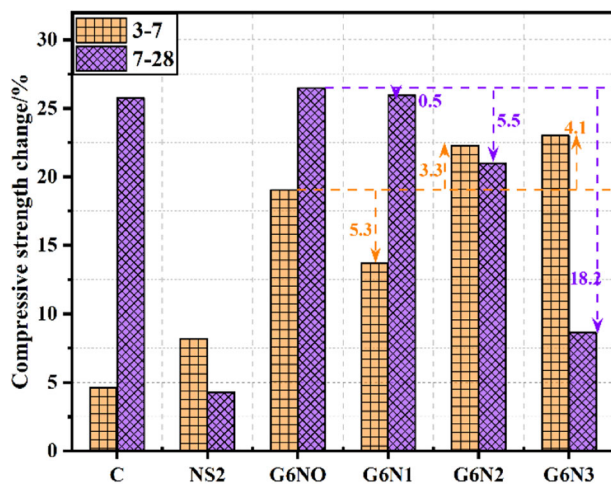
Fig. 4 Compressive strength change evolution of cement paste samples at different curing time intervals (The strength increase of the samples between the ages of 3 to 7 days and 7 to 28 days)

stages. It can be observed that the G6N3 sample exhibited the greatest strength change during the 3–7 days stage, attributed to the synergistic effect of a substantial amount of NS and GBS, and then leading to the formation of more C-S-H gel. The strength change of the G6N1 sample was lower than that of G6N0, as 1 wt% NS was largely consumed during the 3 days, and its later strength increase was less pronounced. The strength change in the C sample was lower than that in the NS samples due to the high reactivity of NS. As the age progressed from 7 days to 28 days, G6N0 demonstrated the highest stage of strength growth. This was because GBS exhibited significant late-stage reactivity [6, 17, 43], and its content was relatively high. With increasing NS dosage, the strength stage growth of G6N1, G6N2, and G6N3 samples all decreased and were lower than that of the G6N0 sample, with reductions of 0.5%, 5.5%, and 18.2%, respectively. These results were associated with the early high reactivity of NS, which generates a significant amount of C-S-H gel encapsulating unhydrated GBS particles and cement minerals, impeding later-stage hydration [42].
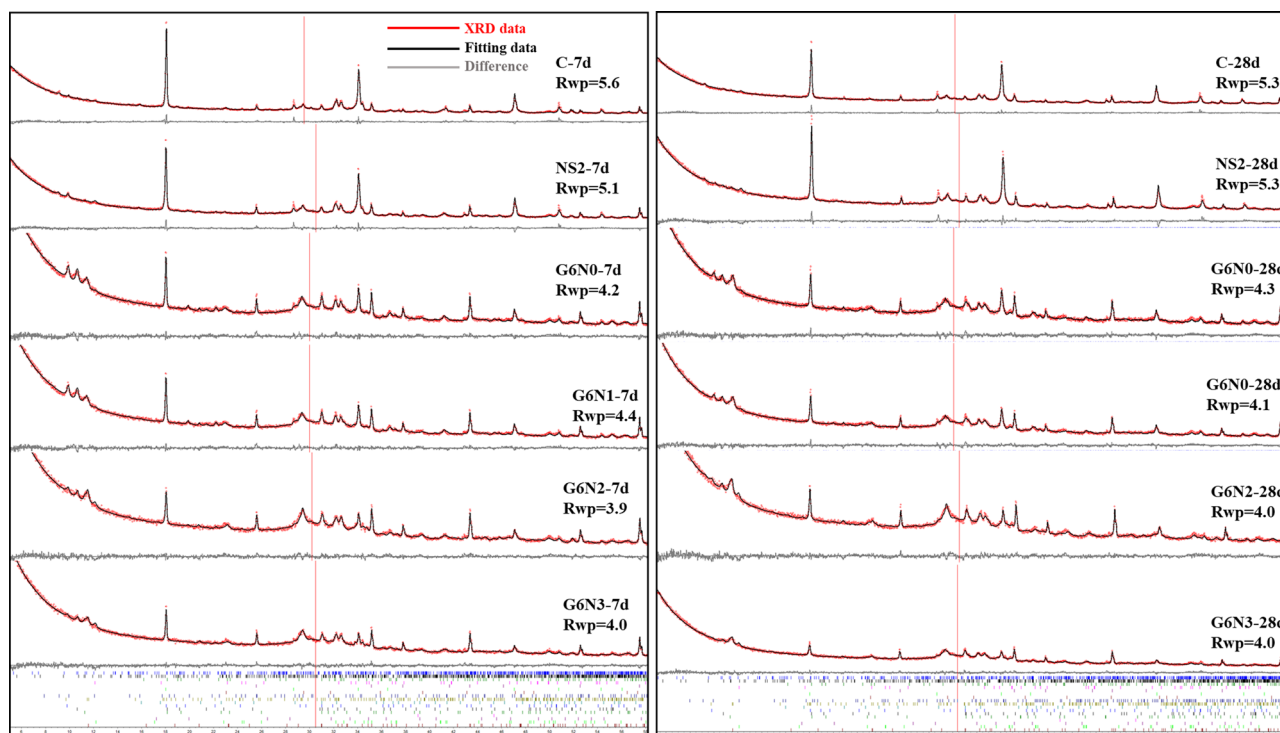
3.2 Quantification of hydration products

To investigate the impact of NS on the hydration products and unhydrated components of high-volume GBS cementitious materials, X-ray diffraction (XRD) tests were conducted on the hydrated mixtures for a specific duration (as shown in Fig. 2), and quantitative analysis was performed using TOPAS software (as shown in Section 2.3.3). XRD analysis was conducted to quantitatively assess the phase composition of the hydration products and the results are shown in Fig. 5a. The fitting data lines and difference after quantitative using TOPAS software are also shown in Fig. 5a, the small fitting

error (difference line and Rwp value) of the quantitative fitting can be observed. The obtained amorphous phase content is illustrated in Fig. 5, indicating that the amorphous phase content of samples with added NS and GBS was higher than that of the C sample. The addition of NS facilitated the hydration and pozzolanic reactions in the composite system, increasing the content of the C-S-H gel. GBS contained a substantial amount of amorphous phase, resulting in a higher content in the 60 wt% GBS composite system. The addition of NS further increased the amorphous phase content in the NS-GBS-cement system, contributing to the strength enhancement observed in Fig. 3. As the curing time increased to 28 days, the amorphous phase content of G6N0 and G6N1, G6N2, and G6N3 samples did not show significant changes or slightly decreased. This was attributed to the pozzolanic reaction of the amorphous phase in GBS during hydration, leading to the formation of amorphous C-S-H gel. The strength enhancement of G6N0 and G6N1, G6N2, and G6N3 samples at 28 days as shown in Fig. 3, confirmed that the late-stage high pozzolanic reactivity of GBS and the formation of predominant strength-contributing phase C-S-H gel.

Figure 6 illustrates the content of unhydrated phases such as C_3S, C_2S, and C_4AF in cement paste samples after various hydration times. For the 7-day age samples, it was evident that the addition of NS significantly reduced the content of unhydrated phases after hydration. The C sample contained 57.2% unhydrated phases, while the NS2 sample contained 39.0, which indicated that NS promoted the hydration of the mineral phase in cement. Substituting cement with GBS reduced the cement content and consequently decreased the unhydrated phase content in the hydration system, with 20.6% unhydrated phases at 7 days. The addition of NS to the GBS cementitious system reduced the unhydrated phase content, with unhydrated phases at 16.7%, 15.7%, and 18.6% for G6N1, G6N2, and G6N3 samples at 7 days, respectively. When the NS content was increased to 3%, the diminishing effect on unhydrated phases weakened, indicating that an excess of NS or hydration products encapsulated the surface of unhydrated particles and hindered hydration. This also confirmed the reason for the strength reduction observed in samples with 3 wt% NS as shown in Fig. 3.

The NS2 sample showed C_3S and C_2S contents of 12.3% and 18.2%, respectively, while the C sample had 17.8% and 25.3% at 7 days. The G6N0 sample had C_3S and C_2S contents of 8.7% and 7.4%. Since GBS replaced 60 wt% of the cement, the calculated percentages of C_3S and C_2S in the GBS blended system at 7 days of hydration should be 7.1% and 10.1%, respectively. This result indicated that the addition of GBS promoted the hydration of C_2S but inhibits the hydration of C_3S. The C_3S and C_2S contents with 7.9%/5.0%, 6.8%/3.9%, and 8.4%/5.1% were presented in G6N1,
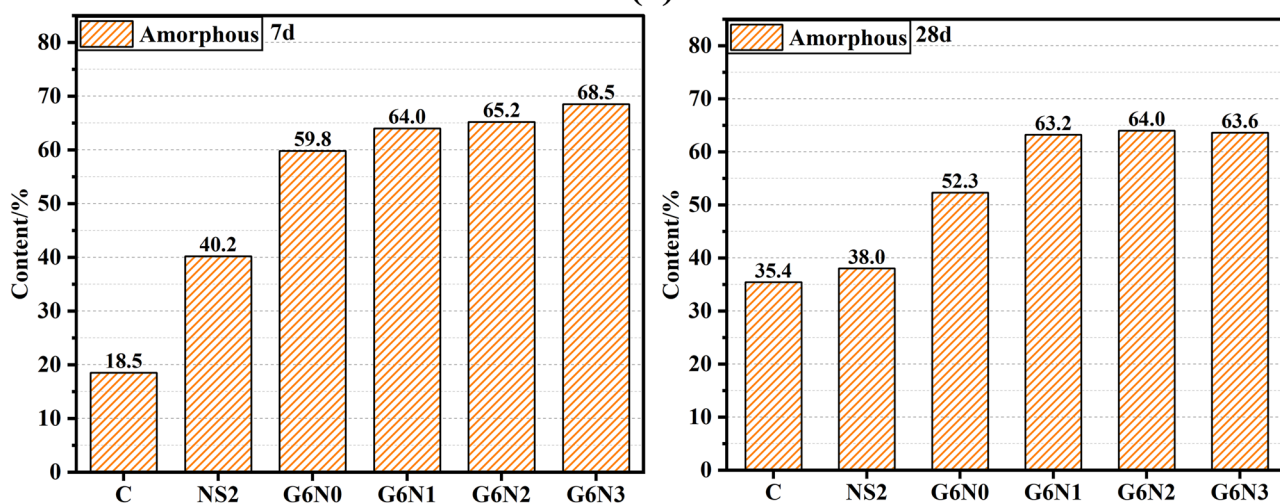
Fig. 5 **a** XRD spectrum and quantification of hydration products of cement paste samples and **b** amorphous content of cement paste samples at different curing age

G6N2, and G6N3 samples, respectively. The NS significantly enhanced the hydration of C_3S and C_2S in 60 wt% GBS cementitious materials. The diminishing effect of 3 wt% NS on promoting the hydration of unhydrated phases was evident, suggesting that excessive NS or hydration products hindered the hydration of unhydrated particles, similar results was shown by other study [41, 42]. Similarly, based on the cement replacement ratio, the G6N0 sample should contain 4.9% C_4AF, but the actual test results show a

content of 3.5%. This indicates that the addition of GBS promotes the hydration of C_4AF. NS simultaneously promoted the hydration of the C_4AF phase in the pure cement system but showed no significant promoting effect on the hydration of the C_4AF phase in the cement-GBS composite system.

At 28 days, the trend of unhydrated phases in all samples was similar to that at 7 days. The C sample had remaining C_3S and C_2S contents of 10.2% and 13.5%, while the
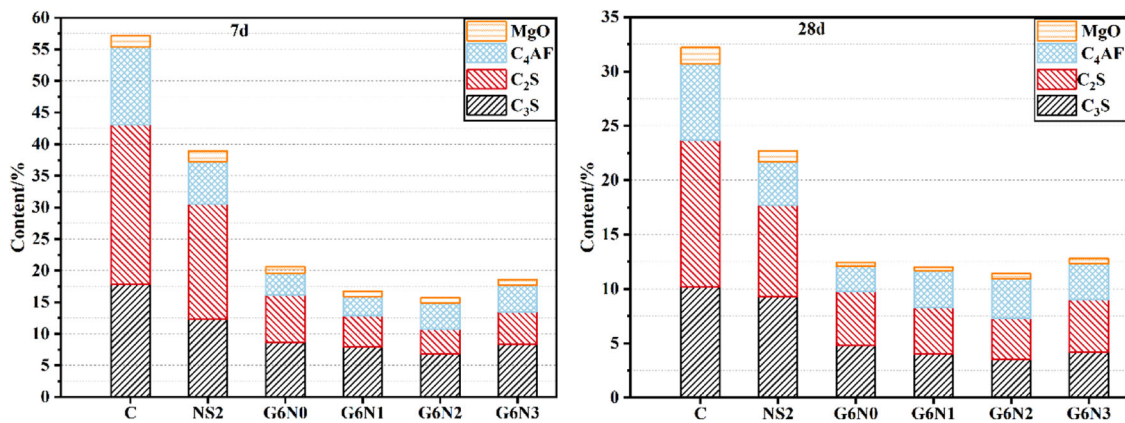
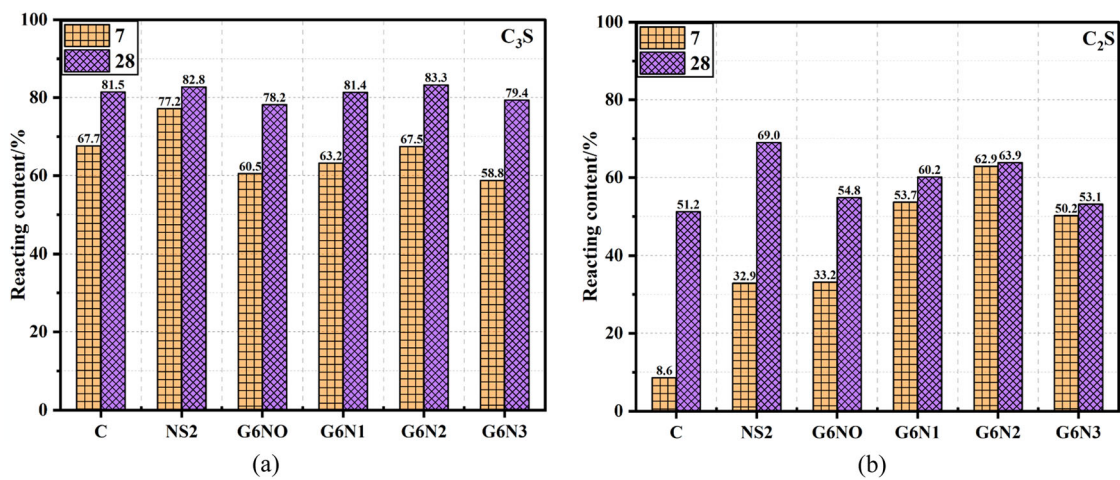Fig. 6 Unhydrated phase content of cement paste samples at different curing age

Fig. 7 Reacting content of (a) C_3S and (b) C_2S in cement paste samples at different curing age

NS2 sample showed 9.3% and 8.4% content. Based on the cement replacement ratio, the G6N0 sample should contain 4.1% and 5.4% fo C_3S and C_2S, but the actual test results show the content of 4.8% and 5.0%. It can be seen that the GBS also showed slightly hydration promoted of C_2S at curing age 28 days. G6N1, G6N2, and G6N3 samples showed the C_3S and C_2S content of 4.0%/4.3%, 3.5%/3.8%, and 4.2%/4.8%, respectively. NS also had a promoting effect on the hydration of C_3S and C_2S in high-volume GBS cementitious materials at 28 days, leading to the formation of more C-S-H gel (as shown in Fig. 5), enhancing the strength and strength development rate of the cement paste (as shown in Fig. 3).

To analyze the reaction quantities of the main hydration phases C_3S and C_2S during the hydration process in different samples, the content of unhydrated C_3S and C_2S in the composite hydration system was calculated based on the replacement amounts of cement by NS and GBS. The percentages of reacted C_3S and C_2S in cement paste with different ratios were calculated for 7-day and 28-day

hydration reactions, as shown in Fig. 7. Figure 7a represents the hydration percentage of C_3S. At 7 days, it was observed that NS significantly increased the hydration percentage of C_3S in the pure cement system. The C sample consumed 67.7% C_3S, while the NS2 sample consumed 77.2% at 7 days. The G6N0 sample had a lower percentage of C_3S consumption than the C sample, indicating that high-volume GBS partially replaced cement does not enhance the hydration of C3S. With the addition of NS in the high GBS cementitious materials, the hydration percentage of C_3S was increased, and it further increased with NS content up to 2 wt%. However, the addition of 3 wt% NS resulted in a significant decrease in the hydration percentage of C_3S, which was explained earlier. The age increased to 28 days, the C_3S reaction percentage increased for all samples. The C sample and NS2 sample showed similar C_3S reaction percentages, consistent with the strength results in Fig. 3. The C_3S consumption percentages for G6N1, G6N2, and G6N3 were all higher than that of the G6N0 sample, indicating that NS continued to promote the late-stage hydration of
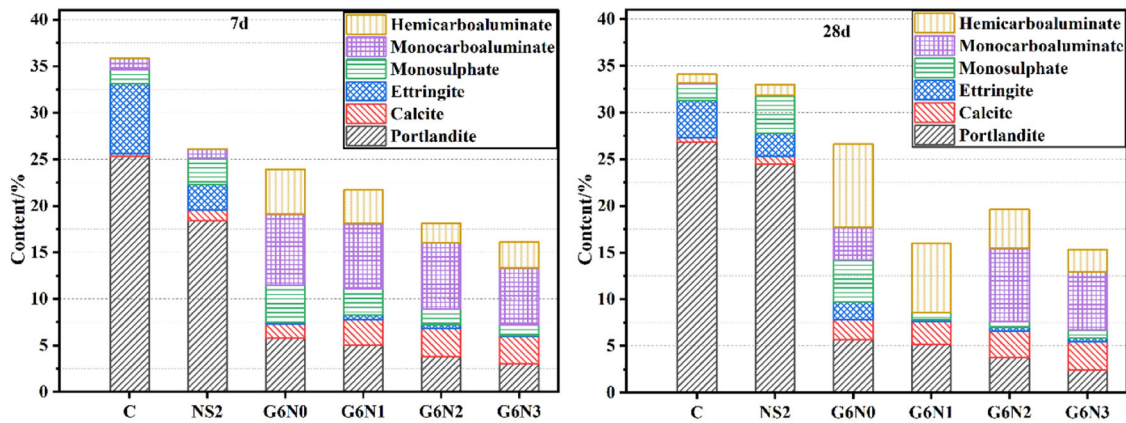
Fig. 8 Hydration phase content of cement paste samples at different curing ages

C_3S in the high-volume GBS cementitious materials. This late-stage hydration effect was not as evident in the pure cement system, which was also revealed by other researchers [21, 22]. From 7 days to 28 days, the difference in C_3S reaction percentage for the C sample was 13.8%, for the NS2 sample was 5.6%, for the G6N0 sample was 17.7%, and for G6N1, G6N2, and G6N3 were 18.2%, 15.8%, and 20.6%, respectively. This also indicated that the addition of NS also had a more significant impact on the late-stage hydration reaction of C_3S in the high-volume GBS cementitious materials.

Figure 8 reveals the content of hydration products at different ages for cement paste samples with various compositions. When cement reacted with water, it generated various amorphous phases such as C-S-H gel and crystalline phases like CH (calcium hydroxide), calcite, ettringite, monosulphate, etc. For the 7-day samples, it can be observed that the C sample contained a significant amount of CH of 25.3%, while its C_3S and C_2S reaction percentages were 67.7% and 8.6%, respectively. In contrast, the NS2 sample exhibited high reaction percentages of C_3S (81.5%) and C_2S (51.2%), with a lower CH content of 18.4%. This suggested that the high pozzolanic reactivity of NS consumed a substantial amount of CH, leading to the formation of C-S-H gel, which proved the high early strength of the NS2 cement paste sample (as shown in Fig. 3). The CH content for the G6N0 sample was 5.8%, while the contents were 5.0%, 3.8%, and 3.0% for G6N1, G6N2, and G6N3 samples, respectively. Similarly, the consumption percentages of C_3S and C_2S in the NS-GBS composite system were higher than those in the G6N0 sample as observed in Fig. 7. This also indicated that NS consumed considerable CH to form C-S-H gel in high-volume GBS cementitious materials, contributing to the early strength enhancement. Some studies [15, 44, 45] also suggest that NS may promote the early pozzolanic reaction of GBS and CH, contributing to improving early strength. The addition of NS reduced the content of ettringite

in the pure cement system after hydration. It increased the content of monosulphate, indicating its retarding influence on the reaction with aluminate minerals and gypsum. This influence was not significant in the high-volume GBS cementitious materials. The hemicarboaluminate and mono-carboaluminate components in the G6N0 sample were significantly higher than those in the C and NS2 samples, suggesting that the addition of high-volume GBS intensified the carbonation of aluminate hydration products. In contrast, the addition of NS reduced this carbonation effect.

At 28 days, the CH content for both the C and NS2 samples significantly increased compared to the content at 7 days, reaching 26.8% and 24.5%, respectively. The CH content in the C and NS2 samples was nearly identical. This was attributed to the fact that the NS was almost completely consumed during the early-age hydration reactions. In the later stages of hydration, it could no longer consume the CH generated during the hydration process. For the G6N0 sample, the CH content was 5.7%, while the contents of 5.2%, 3.8%, and 2.4% resulted from G6N1, G6N2, and G6N3 samples, respectively. These values were similar to the CH content at 7 days, and the CH content for G6N1, G6N2, and G6N3 samples was lower than that for G6N0. This can be attributed to a large amount of GBS in the later stages of hydration, combined with the fact that NS was not completely depleted. As a result, the CH generated during the cement hydration process continued to be consumed. This phenomenon explains why NS still exhibited a significant strength improvement in the later stages of hydration in the high-volume GBS cementitious materials (as shown in Fig. 3). Quantitative results indicated that the calcite content after hydration follows the order: C < NS2 < G6N0 < G6N1 < G6N2 < G6N3. This could be related to the pH of the pore solution and the carbonation resistance of the hydration system, as well as to the transport and gel properties of the hydration system. This reason need further detailed studied.
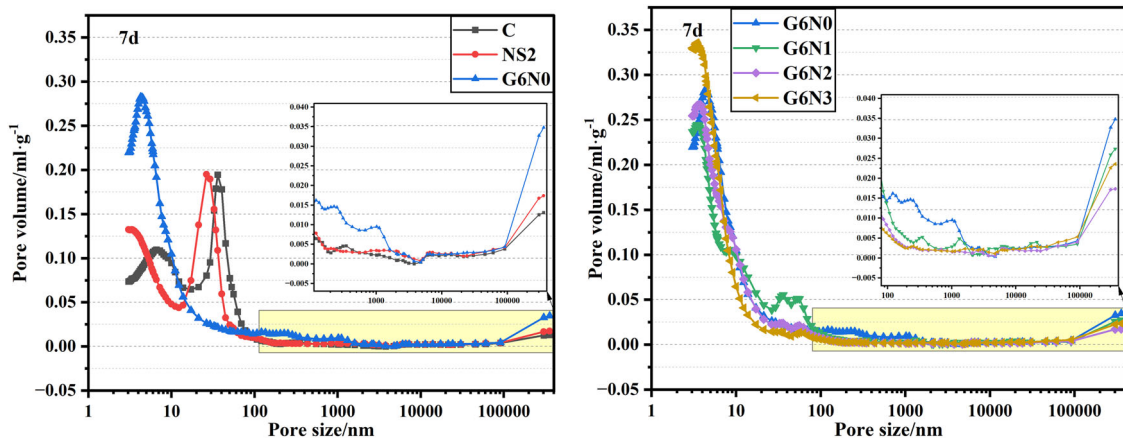
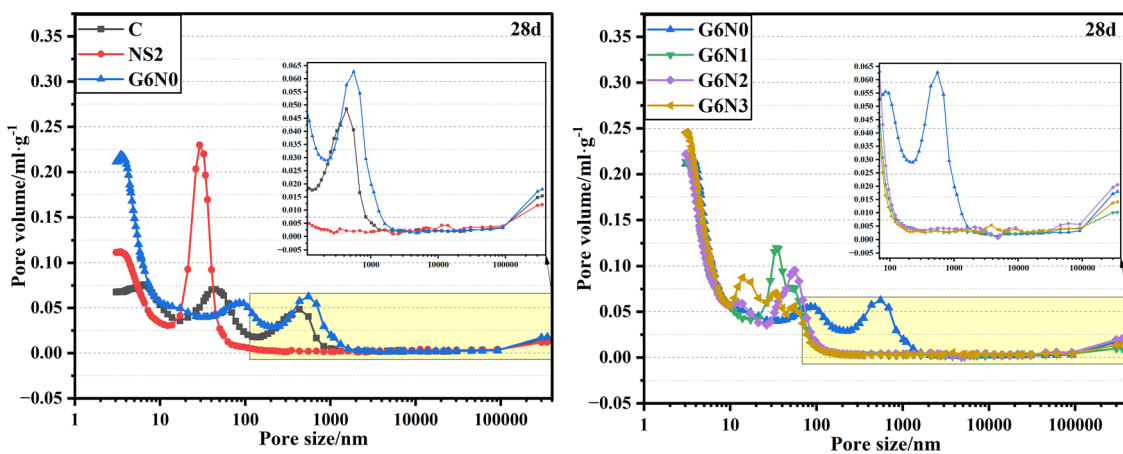Fig. 9 Pore size distribution of cement paste samples at curing age of 7 days

Fig. 10 Pore size distribution of cement paste samples at curing age of 28 days

3.3 Pore structure determination

Figures 9 and 10 shows the pore distribution of cement paste samples with different proportions at 7 days and 28 days of hydration. G6N0 sample exhibited the highest pore volume in the range of greater than 100 μm and between 100 nm and 1 μm at 7 days. Simultaneously, GBS significantly reduced the pore volume in the 10–100 nm range, and there was no peak in the pore distribution within this size range. NS prominently filled pores with diameters less than 10 nm, while the filling effect for pores between 10 nm and 100 nm was not as pronounced. This was attributed to the nanoscale size and high reactivity of NS particles, allowing them to fill smaller pores effectively. Compared to the G6N0 sample, G6N1, G6N2, and G6N3 samples exhibited reduced pore volumes in greater than 100 μm and between 100 nm and 1 μm. The filling effect increased with the increase in NS content. At 28 days of curing, the G6N0 sample showed a significant reduction in pore volume for pores larger than 100 μm, while the

volume of pores between 100 nm and 1 μm increased. With the extended curing time, the C-S-H gel generated by the pozzolanic reaction of GBS filled larger pores and transformed them into smaller pores. The G6N1, G6N2, and G6N3 samples exhibited significantly lower pore volumes in the ranges greater than 100 μm and 100 nm–1 μm than the G6N0 sample. This indicated that NS promoted hydration and pozzolanic reactions at 28 days, enhancing the pore-filling effect. This was also the reason for the higher strength of the 60 wt% GBS sample with NS addition, as shown in Fig. 3.

Figure 11 illustrate the cumulative pore volume for cement pastes with different proportions at various curing ages. For the 7-day samples, NS2 exhibited a higher volume of pores larger than 70 nm than the C sample, while the volume of pores smaller than 70 nm was low. This suggested that NS has a notable effect on filling pores of around 70 nm, with no significant impact on larger pores above 70 nm. The G6N0 sample had a greater volume of pores larger than 60 nm compared to both the C and NS2 samples
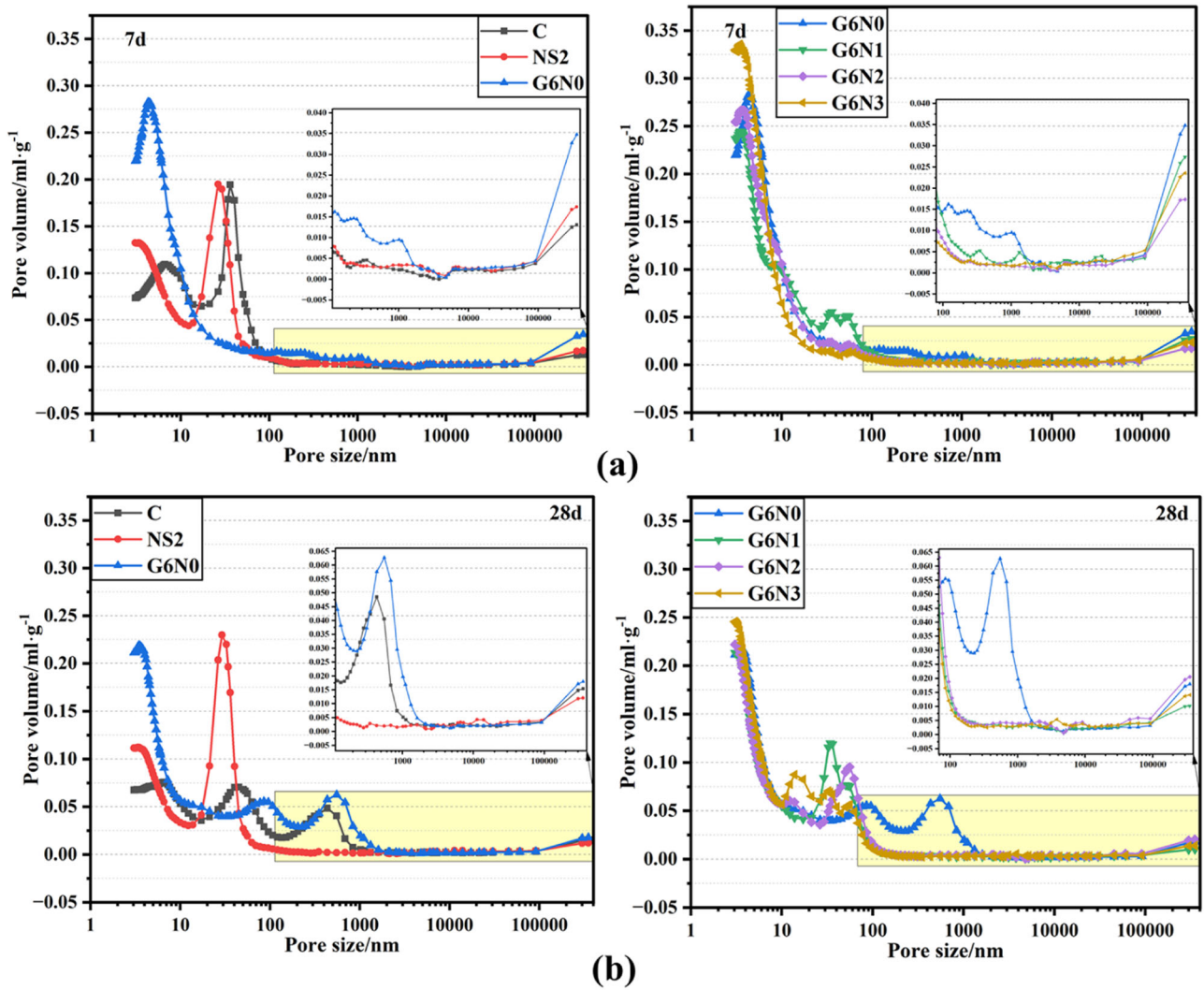
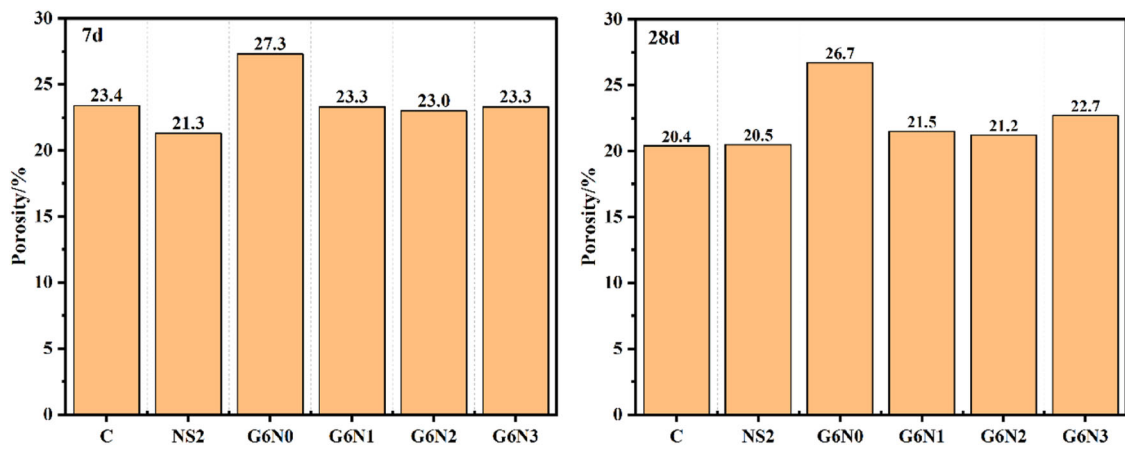**Fig. 11** Cumulative pore volume of cement paste samples at curing age of **a** 7 days and **b** 28 days

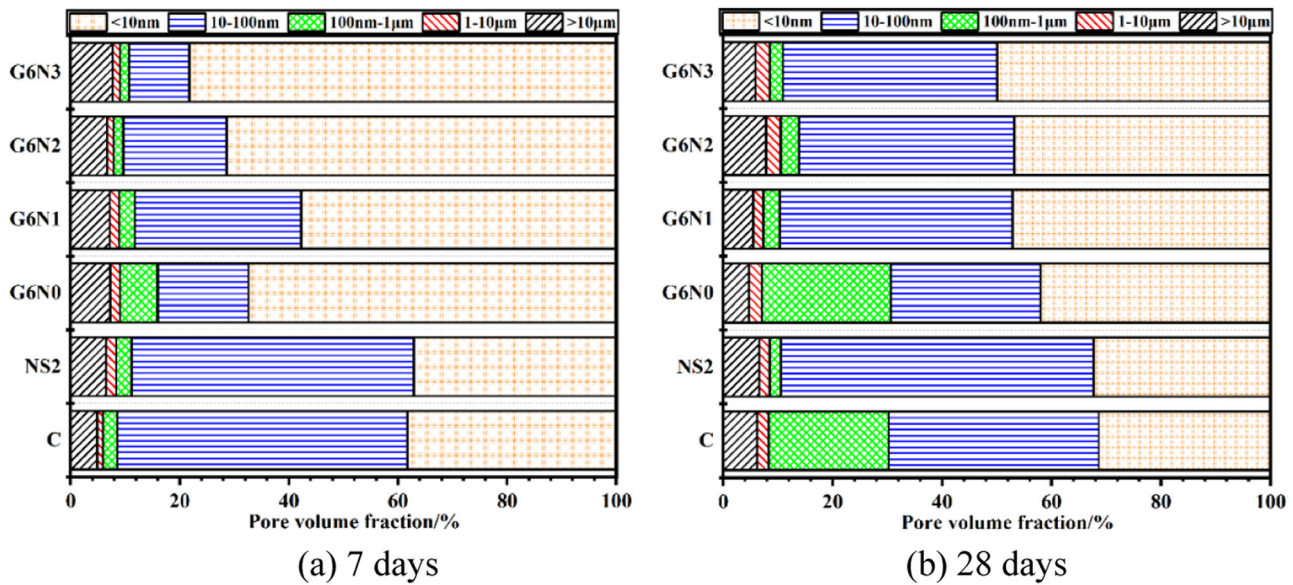**Fig. 12** Porosity of cement paste samples at different curing ages

Fig. 13 Pore fraction of cement paste samples at (**a**) 7 days and (**b**) 28 days

and the highest total pore volume. This implied that the addition of high content of GBS led to a structurally porous and loose matrix, as reflected in Fig. 3 by the low strength of the hardened G6N0 samples. The cumulative volume of pores smaller than 100 nm for G6N1, G6N2, and G6N3 was lower than that of the G6N0 sample. This indicated that the addition of NS reduced the pore volume in the cement-GBS composite system, and its high pozzolanic reactivity and nanoscale size improved the pore-filling effect. For the 28-day samples in Fig. 12, a pattern and trend similar to the 7-day samples were observed. The difference was that the cumulative pore volume curve shifted towards smaller pores, indicating further filling and transforming larger pores into smaller ones.

Figure 12 presents the total porosity of cement pastes with different proportions at various curing ages. It was evident that NS significantly reduced the porosity of the 7-day pure cement cementitious materials, while a high content of GBS increased the porosity of the cement paste samples. NS significantly decreased the porosity of the high-volume GBS cementitious materials, with G6N0 having a porosity of 27.3% and G6N1, G6N2, and G6N3 having porosities of 23.3%, 23.0%, and 23.3%, respectively. It can also be observed that the addition of different volumes of NS had a relatively small impact on the total porosity. As the curing time up to 28 days, the porosity of the NS2 sample became similar to that of the C sample. This suggested that the influence of NS on the pore structure of the pure cementitious system diminished in the later stages of hydration. This was consistent with the effect of NS on hydration products and strength in the later stages of pure cement systems. The total porosity of the G6N0 sample

slightly decreased at 28 days compared to 7 days and still had the highest porosity among all samples. NS continued significantly reducing the porosity of the 60 wt% GBS content cementitious materials at 28 days. This illustrated that NS still had a considerable impact on the pore structure of the high-volume GBS cementitious materials in the later stages of hydration. This consistency aligned with the effect of NS on hydration products and strength in the later stages of hydration in high-volume GBS cementitious materials.

In cementitious materials, pores are typically categorized into gel pores (3–10 nm), mesopores (10–100 nm), capillary pores (100 nm-1 μm), and macropores (>1 μm). Figure 13 illustrates the percentage composition of different types of pores in cementitious materials with varying proportions at different curing ages. At 7 days, the improvement in the pore structure was not very pronounced when comparing NS2 and C samples. The G6N0 sample exhibited a significantly higher percentage of pores larger than 100 nm compared to C and NS2 samples, accompanied by a notable decrease in pores in the 10–100 nm range and a significant increase in pores smaller than 10 nm. G6N1, G6N2, and G6N3 samples show a substantial reduction in the percentage of pores larger than 100 nm relative to the G6N0 sample, with the reduction becoming more pronounced with increasing NS content. NS significantly reduced the percentage of pores from 100 nm to 10 μm in the high-volume GBS cementitious materials. However, the improvement in pores larger than 10 μm was not prominent. During the curing period up to 28 days, NS2 exhibited a significant reduction in pores in the range of 100 nm to 10 μm compared to the C sample, but there was no noticeable effect on pores larger than 10 μm. G6N0 sample showed a decrease in pores larger than 10 μm and an increase
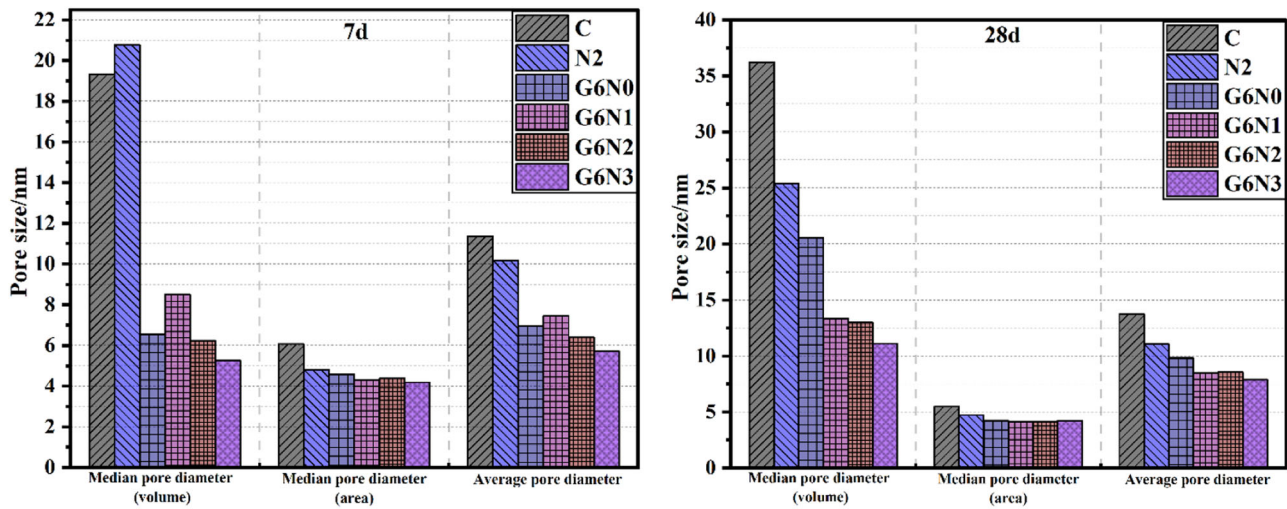
Fig. 14 Median and average pore diameter of cement paste samples at different curing ages
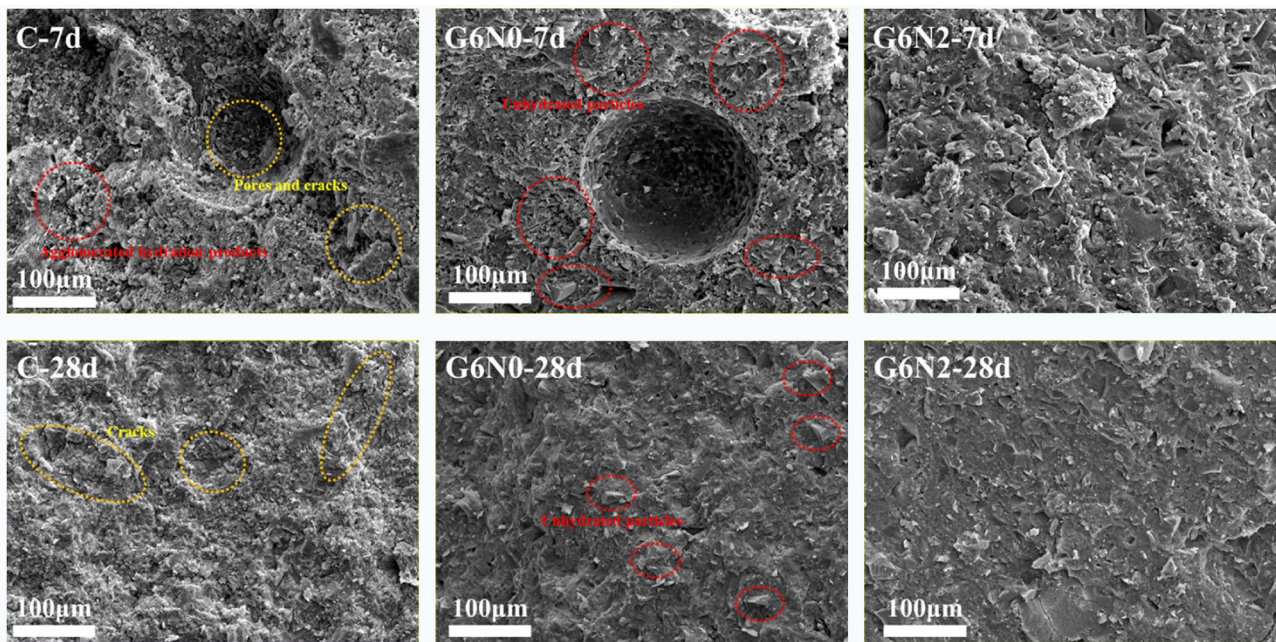

Fig. 15 SEM images of micro-morphology of cement paste hydration at different curing ages

in pores in the range of 10 nm to 1 µm at 28 days relative to 7 days. This was attributed to the late-stage pozzolanic reaction of GBS, generating C-S-H gel to fill larger pores and then transforming them into smaller ones. G6N1, G6N2, and G6N3 samples exhibited a significant reduction in pores larger than 100 nm compared to the G6N0 sample. NS primarily contributed to the reduction in pores in the 100 nm to 10 µm range in high-volume GBS cementitious materials with limited impact on pores larger than 10 µm. These results indicated that NS can enhance the early and late-stage pore structure of high-volume GBS cementitious materials, but its effectiveness in reducing pores larger than 10 µm was limited.

Figure 14 represents cement paste samples' median and average pore diameter at different curing ages. For the 7-day samples, it was evident that adding NS significantly reduced the median and average pore diameter in pure cement and those with high-volume GBS cementitious materials. As the curing period increased to 28 days, the median and average pore diameter for all samples almost uniformly increased. This was attributed to the prolonged hydration time leading to the filling of larger pores by hydration products, transforming them into smaller pores, and consequently causing an increase in pore sizes.

3.4 Morphology

Figure 15 displays SEM micrographs of cement paste samples with different mix proportions at various curing ages. For the 7-day samples, the C sample exhibited numerous pores and cracks, along with aggregates of granular products. The interior walls of the pores also showed many cracks, with loose hydration products filling these cracks. The microstructure of the G6N0 sample was similarly porous, containing many pores, microcracks and numerous unhydrated irregular angular particles. In comparison to the G6N0 sample, the G6N2 sample demonstrated a denser microstructure, with a noticeable reduction in unhydrated GBS particles. Upon curing for 28 days, the C sample's microstructure became denser than the 7-day sample but still showed some microcracks. The microstructure of the G6N0 sample appeared denser with the continued presence of unhydrated irregular angular particles, but these particles were covered with more gel-like material. The G6N2 sample showed a significant reduction in unhydrated particles and denser structure compared to G6N0.

4 Conclusions

This study investigated the influence of nano-silica on the macroscopic mechanical properties and microscopic structure of cementitious materials with a high volume of ground granulated blast furnace slag. Tests and analyses were conducted on the cement paste's strength, hydration product, pore structure, and microstructure. The following conclusions were drawn through comparative discussions on the performance of specimens with different curing ages and various NS dosages.

1. A notable decrease in strength was noted in high-volume GBS cement paste. NS exhibited a remarkable enhancement in the early strength (at 3 and 7 days) of both pure cement and high volume-GBS composite systems. The strength enhancement by NS in pure cement even demonstrated adverse effects on strength development during the 28-day hydration period. However, the beneficial influence of NS on the strength of high-volume GBS-contained samples remained evident at 28 days of age.

2. NS facilitated the hydration of C3S and C2S in blended cementitious systems. The enhancement in the hydration percentage of C2S was particularly pronounced, especially in high-volume GBS cementitious materials. In high-volume GBS cementitious materials, NS continues to consume CH and participate in the hydration reaction at later ages, this phenomenon that diminishes in pure cement systems.

Simultaneously, NS mitigated the carbonation of aluminum phase hydration products in high-volume GBS cementitious materials.

3. GBS significantly reduced the pore volume in the 10–100 nm range, while NS prominently filled pores with diameters smaller than 10 nm. Adding NS to high-volume GBS cementitious materials further decreased the pore volume in the ranges of >100 μm and 100 nm-1 μm. In the later stages of hydration, the influence of NS on the pore structure of the pure cementitious system diminished, whereas it remained prominent in high-volume GBS cement paste.

4. In high-volume GBS cement paste, the enhancement of strength and the promotion of C3S and C2S hydration increased with higher additions of NS at 1 wt% and 2 wt%. However, this enhancement and promotion effect diminished when the NS dosage increased to 3 wt%. This suggests that an optimal NS dosage exists, and more is not necessarily better.

Author contributions Qinqiang Wang: Conceptualization; Methodology; Investigation; Data curation, Writing-Original draft preparation. Kangbing Ma: Supervision. Tao Liu: Investigation; Writing- Editing.

Compliance with ethical standards

Conflict of interest The authors declare no competing interests.

References

1. Giergiczny Z (2019) Fly ash and slag. Cement Concr Res 124. https://doi.org/10.1016/j.cemconres.2019.105826

2. Lothenbach B, Scrivener K, Hooton RD (2011) Supplementary cementitious materials. Cem Concr Res 41(12):1244–1256. https://doi.org/10.1016/j.cemconres.2010.12.001

3. Supriya, Chaudhury R, Sharma U, Thapliyal PC, Singh LP (2023) Low-CO2 emission strategies to achieve net zero target in cement sector. J Cleaner Prod 417. https://doi.org/10.1016/j.jclepro.2023.137466

4. Wang HY, Wang WC, Wang JC, Chen YW (2021) Evaluation of the engineering properties and durability of mortar produced using ground granulated blast-furnace slag and stainless steel reduced slag. Constr Build Mater 280. https://doi.org/10.1016/j.conbuildmat.2021.122498

5. Vigneshkumar A, Freeda Christy C, Muthukannan M, Maheswaran M, Arunkumar K, Kanniga Devi R (2024) Experimental investigations on fresh and mechanical properties of fly ash and ground granulated blast furnace slag self-compacting geopolymer concrete. Mater Today Proc. https://doi.org/10.1016/j.matpr.2024.01.051

6. Ozturk M, Karaaslan M, Akgol O, Sevim UK (2020) Mechanical and electromagnetic performance of cement based composites containing different replacement levels of ground granulated blast furnace slag, fly ash, silica fume and rice husk ash. Cement Concr Res 136. https://doi.org/10.1016/j.cemconres.2020.106177

7. Özbay E, Erdemir M, Durmuş Hİ (2016) Utilization and efficiency of ground granulated blast furnace slag on concrete properties – a review. Constr Build Mater 105:423–434. https://doi.org/10.1016/j.conbuildmat.2015.12.153

8. Aprianti E, Shafigh P, Zawawi R, Abu Hassan ZF (2016) Introducing an effective curing method for mortar containing high volume cementitious materials. Constr Build Mater 107:365–377. https://doi.org/10.1016/j.conbuildmat.2015.12.100

9. Taylor R, Richardson IG, Brydson RMD (2010) Composition and microstructure of 20-year-old ordinary Portland cement–ground granulated blast-furnace slag blends containing 0 to 100% slag. Cem Concr Res 40(7):971–983. https://doi.org/10.1016/j.cemconres.2010.02.012

10. Song HW, Saraswathy V (2006) Studies on the corrosion resistance of reinforced steel in concrete with ground granulated blast-furnace slag-an overview. J Hazard Mater 138(2):226–233. https://doi.org/10.1016/j.jhazmat.2006.07.022

11. Duraman SB, Richardson IG (2020) Microstructure & properties of steel-reinforced concrete incorporating Portland cement and ground granulated blast furnace slag hydrated at 20 °C. Cement Concr Res 137. https://doi.org/10.1016/j.cemconres.2020.106193

12. Tang Q, Ma Z, Wu H, Wang W (2020) The utilization of eco-friendly recycled powder from concrete and brick waste in new concrete: a critical review. Cement Concr Compos 114. https://doi.org/10.1016/j.cemconcomp.2020.103807

13. Choi YC, Kim J, Choi S (2017) Mercury intrusion porosimetry characterization of micropore structures of high-strength cement pastes incorporating high volume ground granulated blast-furnace slag. Constr Build Mater 137:96–103. https://doi.org/10.1016/j.conbuildmat.2017.01.076

14. Li G, Zhang A, Song Z, Liu S, Zhang J (2018) Ground granulated blast furnace slag effect on the durability of ternary cementitious system exposed to combined attack of chloride and sulfate. Constr Build Mater 158:640–648. https://doi.org/10.1016/j.conbuildmat.2017.10.062

15. Xu Z, Gao J, Zhao Y, Li S, Guo Z, Luo X, Chen G (2022) Promoting utilization rate of ground granulated blast furnace slag (GGBS): Incorporation of nanosilica to improve the properties of blended cement containing high volume GGBS. J Cleaner Product 332. https://doi.org/10.1016/j.jclepro.2021.130096

16. Yang Y, Zhan B, Wang J, Zhang Y, Duan W (2020) Damage evolution of cement mortar with high volume slag exposed to sulfate attack. Constr Build Mater 247. https://doi.org/10.1016/j.conbuildmat.2020.118626

17. Rashad AM (2018) An overview on rheology, mechanical properties and durability of high-volume slag used as a cement replacement in paste, mortar and concrete. Constr Build Mater 187:89–117. https://doi.org/10.1016/j.conbuildmat.2018.07.150

18. Xu G, Tian Q, Miao J, Liu J (2017) Early-age hydration and mechanical properties of high volume slag and fly ash concrete at different curing temperatures. Constr Build Mater 149:367–377. https://doi.org/10.1016/j.conbuildmat.2017.05.080

19. Guo Z, Xu Z, Liu C, Gao J, Luo X, Li S (2023) New insights into the effects of nanosilica on transmission properties and pore structure in high-volume blast furnace slag cementitious materials. Constr Build Mater 404. https://doi.org/10.1016/j.conbuildmat.2023.133181

20. Sanjuán MÁ, Estévez E, Argiz C, Barrio DD (2018) Effect of curing time on granulated blast-furnace slag cement mortars carbonation. Cem Concr Compos 90:257–265. https://doi.org/10.1016/j.cemconcomp.2018.04.006

21. Barbhuiya GH, Moiz MA, Hasan SD, Zaheer MM (2020) Effects of the nanosilica addition on cement concrete: a review. Mater Today Proc 32:560–566. https://doi.org/10.1016/j.matpr.2020.02.143

22. Du H, Pang SD (2019) High performance cement composites with colloidal nano-silica. Constr Build Mater 224:317–325. https://doi.org/10.1016/j.conbuildmat.2019.07.045

23. Rupasinghe M, San Nicolas R, Mendis P, Sofi M, Ngo T (2017) Investigation of strength and hydration characteristics in nano-silica incorporated cement paste. Cem Concr Compos 80:17–30. https://doi.org/10.1016/j.cemconcomp.2017.02.011

24. Norhasri MSM, Hamidah MS, Fadzil AM (2017) Applications of using nano material in concrete: a review. Constr Build Mater 133:91–97. https://doi.org/10.1016/j.conbuildmat.2016.12.005

25. Li LG, Huang ZH, Zhu J, Kwan AKH, Chen HY (2017) Synergistic effects of micro-silica and nano-silica on strength and microstructure of mortar. Constr Build Mater 140:229–238. https://doi.org/10.1016/j.conbuildmat.2017.02.115

26. Kawashima S, Hou P, Corr DJ, Shah SP (2013) Modification of cement-based materials with nanoparticles. Cem Concr Compos 36:8–15. https://doi.org/10.1016/j.cemconcomp.2012.06.012

27. Singh LP, Karade SR, Bhattacharyya SK, Yousuf MM, Ahalawat S (2013) Beneficial role of nanosilica in cement based materials – a review. Constr Build Mater 47:1069–1077. https://doi.org/10.1016/j.conbuildmat.2013.05.052

28. Hou P, Kawashima S, Kong D, Corr DJ, Qian J, Shah SP (2013) Modification effects of colloidal nanoSiO2 on cement hydration and its gel property. Compos Part B Eng 45(1):440–448. https://doi.org/10.1016/j.compositesb.2012.05.056

29. Jo B-W, Kim C-H, Tae G-h, Park J-B (2007) Characteristics of cement mortar with nano-SiO2 particles. Constr Build Mater 21(6):1351–1355. https://doi.org/10.1016/j.conbuildmat.2005.12.020

30. Madani H, Bagheri A, Parhizkar T (2012) The pozzolanic reactivity of monodispersed nanosilica hydrosols and their influence on the hydration characteristics of Portland cement. Cem Concr Res 42(12):1563–1570. https://doi.org/10.1016/j.cemconres.2012.09.004

31. Hou P, Guo Z, Li Q, Zhang X, Liu J, Yang S, Cheng X, Kumar R, Srinivasaraonaik B, Singh LP (2019) Comparison study on the sulfate attack resistivity of cement-based materials modified with nanoSiO2 and normal SCMs: pore structure and phase composition. Constr Build Mater 228. https://doi.org/10.1016/j.conbuildmat.2019.116764

32. Liu X, Feng P, Li W, Geng G, Huang J, Gao Y, Mu S, Hong J (2021) Effects of pH on the nano/micro structure of calcium silicate hydrate (C-S-H) under sulfate attack. Cement Concrete Res 140. https://doi.org/10.1016/j.cemconres.2020.106306

33. Huang Q, Zhu X, Zhao L, Zhao M, Liu Y, Zeng X (2020) Effect of nanosilica on sulfate resistance of cement mortar under partial immersion. Constr Build Mater 231. https://doi.org/10.1016/j.conbuildmat.2019.117180

34. Guo Z, Wang Y, Hou P, Shao Y, Zuo X, Li Q, Xie N, Cheng X (2019) Comparison study on the sulfate attack resistivity of cement-based materials modified with nanoSiO2 and conventional SCMs: mechanical strength and volume stability. Constr Build Mater 211:556–570. https://doi.org/10.1016/j.conbuildmat.2019.03.235

35. Guo Z, Hou P, Huang S, Xie N, Cheng X, Singh LP, Valeriya S, Viktoriya N (2018) Surface treatment of concrete with tetraethyl orthosilicate, Na2SiO3 and silane: comparison of their effects on durability. Ceram-Silik 62(4):332–341. https://doi.org/10.13168/cs.2018.0029

36. Singh LP, Bhattacharyya SK, Shah SP, Mishra G, Sharma U (2016) Studies on early stage hydration of tricalcium silicate incorporating silica nanoparticles: Part II. Constr Build Mater 102:943–949. https://doi.org/10.1016/j.conbuildmat.2015.05.084

37. Singh LP, Bhattacharyya SK, Shah SP, Mishra G, Ahalawat S, Sharma U (2015) Studies on early stage hydration of tricalcium silicate incorporating silica nanoparticles: Part I. Constr Build Mater 74:278–286. https://doi.org/10.1016/j.conbuildmat.2014.08.046

38. Dolado JS, Campillo I, Erkizia E, Ibáñez JA, Porro A, Guerrero A, Goñi S (2007) Effect of nanosilica additions on belite cement pastes held in sulfate solutions. J Am Ceram Soc 0 (0):3973–3976. https://doi.org/10.1111/j.1551-2916.2007.02034.x

39. Hou P, Wang X, Zhao P, Wang K, Kawashima S, Li Q, Xie N, Cheng X, Shah SP (2020) Physicochemical effects of nanosilica on C3A/C3S hydration. J Am Ceram Soc 103(11):6505–6518. https://doi.org/10.1111/jace.17364

40. Ground granulated blast furnace slag used for cement and concrete. GBT 18046-2008

41. Land G, Stephan D (2015) Controlling cement hydration with nanoparticles. Cem Concr Compos 57:64–67. https://doi.org/10.1016/j.cemconcomp.2014.12.003

42. Hou P, Wang K, Qian J, Kawashima S, Kong D, Shah SP (2012) Effects of colloidal nanoSiO2 on fly ash hydration. Cem Concr Compos 34(10):1095–1103. https://doi.org/10.1016/j.cemconcomp.2012.06.013

43. Shen D, Jiao Y, Gao Y, Zhu S, Jiang G (2020) Influence of ground granulated blast furnace slag on cracking potential of high performance concrete at early age. Constr Build Mater 241. https://doi.org/10.1016/j.conbuildmat.2019.117839

44. Xu Z, Guo Z, Zhao Y, Li S, Luo X, Chen G, Liu C, Gao J (2023) Hydration of blended cement with high-volume slag and nano-silica. J Build Eng 64. https://doi.org/10.1016/j.jobe.2022.105657

45. Liu X, Hou P, Chen H (2021) Effects of nanosilica on the hydration and hardening properties of slag cement. Constr Build Mater 282. https://doi.org/10.1016/j.conbuildmat.2021.122705